

Workspace Analysis and Optimal Design of Cable-Driven Parallel Robots via Auxiliary Counterbalances^{*}

Ronghuai Qi^{*}, Hamed Jamshidifar, Amir Khajepour

Department of Mechanical and Mechatronics Engineering, University of Waterloo, Waterloo, ON N2L 3G1, Canada

Abstract

Cable-driven parallel robots (CDPRs) are widely investigated and applied in the worldwide; however, traditional configurations make them to be limited in reaching their maximum workspace due to constraints such as the maximum allowable tensions of cables. In this paper, we introduce auxiliary counterbalances to tackle this problem and focus on workspace analysis and optimal design of CDPRs with such systems. Besides, kinematics, dynamics, and parameters optimization formulas and algorithm are provided to maximize the reachable workspace of CDPRs. Case studies for different configurations are presented and discussed. Numerical results suggest the effectiveness of the aforementioned approaches, and the obtained parameters can also be applied for actual CDPRs design.

Keywords: Cable-driven parallel robot, auxiliary counterbalances, workspace optimization, mechanism design.

1. Introduction

Cable-driven parallel robots (CDPRs) are an important type of industrial robot. Their configurations usually bear a resemblance to parallel manipulators. In these robots, rigid links are replaced with cables (e. g., a typical CDPR - NIST RoboCrane in [1, 2]) in order to reduce their weight. It also eliminates the need for these revolute joints. These features allow the mobile platform to reach high motion accelerations in large workspaces. Due to these benefits, CDPRs are widely used in industry, rehabilitation, and other fields. For instance, researchers [3, 4, 5] developed a CDPR, where the mobile platform is driven by two sets of upper cables and two sets of lower cables. They focused on the in-plane vibration control of the CDPR. However, owing to the effect of gravity on the cable-driven mobile platforms, conventional CDPRs cannot reach the top positions of the desired workspace since cable tensions may reach their maximum allowable values, and this problem widely exists in CDPRs.

To overcome the workspace limitation problem, researchers [4, 5, 6, 7, 8, 9, 10, 11, 12, 13, 14, 15] have attempted to mount manipulators or tools on the CDPRs. Literature shows that existing research and applications prefer to affix a robot arm upside down to the bottom of a CDPR's platform [8, 9, 10, 11, 12, 13, 14, 15]. But this configuration cannot effectively improve the reachable workspace on the top space. The authors [6, 7] developed hybrid cable-driven robots (HCDRs), in which robot arms are mounted on the top of the CDPRs to deal with this problem. The experimental CDPR was based on the existing planar CDPR [3], in which a mobile platform is driven by two sets of upper cables and two sets of lower cables. Jamshidifar [5] used this platform for studying the rigid body and in-plane vibration control of CDPR. Rushton [16] introduced two pendulums to eliminate out-of-plane vibrations. The HCDRs can overcome the shortcomings of CDPRs and serial robots as well as aggregate their advantages. When a serial robot is mounted on a mobile platform, the two constitute a new coupled system, leading some new problems, e.g., only controlling the mobile platform or the serial robot may not guarantee the position accuracy of the end-effector. Besides, another major challenge in the utilization of these systems is maintaining the appropriate cable tensions and stiffness for the

^{*}This work was supported in part by the Natural Sciences and Engineering Research Council of Canada (NSERC).

^{*}Corresponding author

Email addresses: r5qi@uwaterloo.ca (Ronghuai Qi), hjamshid@uwaterloo.ca (Hamed Jamshidifar), a.khajepour@uwaterloo.ca (Amir Khajepour)

robot. This requires the development of kinematic and dynamic models, stiffness optimization, and controllers for HCDRs. Some research has been carried out to solve these problems: for kinematic and dynamic modeling, existing research mainly focuses on rigid serial robots [17] and rigid/flexible parallel robots [3, 5, 18, 19, 20, 21, 22, 23, 24]. Some useful methods were studied to solve the redundancy and stiffness optimization problems, such as the minimum 2-norm of cable tensions [3, 5] and stiffness maximization in the softest direction [5]. However, the former one cannot make all cable tensions be positive; the latter one is complicated. Additionally, the moving robot arm also generates reaction forces acting on the mobile platform, resulting in mobile platform vibrations. In short, it is challenging to achieve the goal of minimizing the vibrations and increasing the position accuracy of the end-effector simultaneously. Hence, mounting manipulators and tools on the CDPRs makes the overall system complicated and results in vibrations and other problems above. These problems do not contribute to the improvement of the workspace.

Regarding the workspace analysis and optimal design, researchers developed numerical generation methods. For instance, Pham et al. [25] proposed a simplex search method to obtain the available workspace, but the computation efficiency is not high. Taking a planar CDPR as the object, Li [26] and Bolboli et al. [27] developed GA-based methods to study the optimal design and workspace analysis, but whether the design methodology can be extended to other CDPRs are still ongoing. Tang [28] proposed a workspace quality index to analyze the workspace. Pusey [29] et al. studied the design and workspace analysis of a 6-6 CDPR by using the set of points of the workspace volume. Merlet [30] investigated the workspace of suspended CDPRs using straight-line cables, straight-line linear elastic cables, and sagging cables. But the author did not provide a clear analytical solution to determine the border equation for sagging cable since it was much more complicated in this situation. However, such techniques cannot tackle the problems for the configuration in this paper. Although the authors in [31] studied the effects on the wrench-feasible workspace of CDPRs by adding springs, they provided an optimization equation to find feasible spring parameters, but not the optimal parameters of CDPRs. Besides, they used the existing null space of the structure matrix method in [32] to solve the workspace optimization problem, i.e., they didn't contribute to the improvement of the workspace optimization algorithm. The numerical results showed that adding springs on a planar CDPR didn't increase (i.e., just change) the reachable workspace. In order to tackle the problems above, in this paper, we present workspace analysis and optimal design of CDPRs via auxiliary counterbalances. The main contributions are as follows:

1. Auxiliary counterbalance systems are introduced to increase the reachable workspace of CDPRs.
2. Modeling and parameters optimization approaches for CDPRs workspace extension are investigated with such systems.
3. Different configurations are proposed and compared for optimal design.
4. Case studies are conducted to verify the effectiveness of aforementioned approaches.

The rest of this paper is organized as below: in Section 2, we focus on system modeling, including kinematics and dynamics. In Section 3, we develop a new workspace analysis method. Then, in Section 4, we use specific CDPR numerical results to verify the proposed methods. Finally, in Section 5, we summarize the conclusions and further work.

2. Modeling

2.1. General Configuration

Consider a general cable-driven parallel robot, i.e., a moving platform that is actuated by multi-cables (see Figure 1) and all cables are assumed to be straight and massless. To increase the reachable workspace, we introduce auxiliary counterbalances. The configuration and coordinate assignment of the CDPR with a genetic auxiliary counterbalance system are shown in Figure 1, in which the CDPR has n ($n \in \mathbb{N}$) driven cables (actuated by active winches), and m ($m \in \mathbb{N}$) cables (actuated by a counterbalance system) connected to the auxiliary fixed pulleys. The genetic auxiliary counterbalance system consists of multi fixed pulleys and a counterweight, in which the counterweight can be replaced by a hydraulic system or other similar counterbalances. In this paper, we focus on using the counterweight for modeling and analysis. \mathbf{a}_i ($\{\forall i \in \mathbb{N} : 1 \leq i \leq n\}$) and \mathbf{f}_j ($\{\forall j \in \mathbb{N} : 1 \leq j \leq m\}$) are position vectors of the i -th cable and j -th cable, respectively, with respect to the global coordinate frame $X_0Y_0Z_0$. \mathbf{r}_i and \mathbf{c}_j are body-fixed

where \mathbf{d}_j and d_j represent the j -th cable length vector and cable length, respectively. $\hat{\mathbf{v}}_j$ denotes the unit vector of the j -th cable connected to the corresponding auxiliary fixed pulley. Differentiating (1) and (4), we get

$$-\dot{l}_i \hat{\mathbf{u}}_i - \omega_i \times (l_i \hat{\mathbf{u}}_i) = \dot{\mathbf{p}} + \omega_m \times \mathbf{r}_i \quad (7)$$

$$\dot{l}_i = -\hat{\mathbf{u}}_i (\dot{\mathbf{p}} + \omega_m \times \mathbf{r}_i + \omega_i \times (l_i \hat{\mathbf{u}}_i)) \quad (8)$$

$$= -\begin{bmatrix} \hat{\mathbf{u}}_i^T & (\mathbf{r}_i \times \hat{\mathbf{u}}_i)^T \end{bmatrix} \begin{bmatrix} \dot{\mathbf{p}} \\ \omega_m \end{bmatrix}, \quad (9)$$

and then, the vector of cable length velocity can be described as

$$\begin{bmatrix} \dot{l}_1 \\ \dot{l}_2 \\ \vdots \\ \dot{l}_n \end{bmatrix} = - \underbrace{\begin{bmatrix} \hat{\mathbf{u}}_1^T & (\mathbf{r}_1 \times \hat{\mathbf{u}}_1)^T \\ \hat{\mathbf{u}}_2^T & (\mathbf{r}_2 \times \hat{\mathbf{u}}_2)^T \\ \cdots & \cdots \\ \hat{\mathbf{u}}_n^T & (\mathbf{r}_n \times \hat{\mathbf{u}}_n)^T \end{bmatrix}}_{\triangleq \mathbf{J}_l} \begin{bmatrix} \dot{\mathbf{p}} \\ \omega_m \end{bmatrix}, \quad (10)$$

where ω_i represents the angle velocity of the i -th cable, $\dot{\mathbf{p}}$ and ω_m are linear and angle velocities of the mobile platform. \mathbf{J}_l denotes the Jacobian matrix of the CDPR. Similarly, for the auxiliary fixed pulleys, we also have

$$\dot{d}_j = -\begin{bmatrix} \hat{\mathbf{v}}_j^T & (\mathbf{c}_j \times \hat{\mathbf{v}}_j)^T \end{bmatrix} \begin{bmatrix} \dot{\mathbf{p}} \\ \omega_m \end{bmatrix}, \quad (11)$$

$$\begin{bmatrix} \dot{d}_1 \\ \dot{d}_2 \\ \vdots \\ \dot{d}_m \end{bmatrix} = - \underbrace{\begin{bmatrix} \hat{\mathbf{v}}_1^T & (\mathbf{c}_1 \times \hat{\mathbf{v}}_1)^T \\ \hat{\mathbf{v}}_2^T & (\mathbf{c}_2 \times \hat{\mathbf{v}}_2)^T \\ \cdots & \cdots \\ \hat{\mathbf{v}}_m^T & (\mathbf{c}_m \times \hat{\mathbf{v}}_m)^T \end{bmatrix}}_{\triangleq \mathbf{J}_d} \begin{bmatrix} \dot{\mathbf{p}} \\ \omega_m \end{bmatrix}, \quad (12)$$

where \dot{d}_j means the j -th cable length velocity. \mathbf{J}_d denotes the Jacobian matrix resulting from the auxiliary fixed pulleys. Finally, combining (13) and (12), we can obtain

$$\begin{bmatrix} \dot{l}_1 \\ \dot{l}_2 \\ \vdots \\ \dot{l}_n \\ \dot{d}_1 \\ \dot{d}_2 \\ \vdots \\ \dot{d}_m \end{bmatrix} = - \underbrace{\begin{bmatrix} \hat{\mathbf{u}}_1^T & (\mathbf{r}_1 \times \hat{\mathbf{u}}_1)^T \\ \hat{\mathbf{u}}_2^T & (\mathbf{r}_2 \times \hat{\mathbf{u}}_2)^T \\ \cdots & \cdots \\ \hat{\mathbf{u}}_n^T & (\mathbf{r}_n \times \hat{\mathbf{u}}_n)^T \\ \hat{\mathbf{v}}_1^T & (\mathbf{c}_1 \times \hat{\mathbf{v}}_1)^T \\ \hat{\mathbf{v}}_2^T & (\mathbf{c}_2 \times \hat{\mathbf{v}}_2)^T \\ \cdots & \cdots \\ \hat{\mathbf{v}}_m^T & (\mathbf{c}_m \times \hat{\mathbf{v}}_m)^T \end{bmatrix}}_{\triangleq \mathbf{J}} \begin{bmatrix} \dot{\mathbf{p}} \\ \omega_m \end{bmatrix}, \quad (13)$$

where \mathbf{J} is the Jacobian matrix of the whole system.

2.3. Dynamics

Using the obtained results in Subsection 2.2 and Newton-Euler's law, we can derive the equations of motion of the whole system as

$$\begin{aligned}
\begin{bmatrix} m_m \dot{\mathbf{v}}_m \\ \mathbf{I}_m \dot{\boldsymbol{\omega}}_m + \boldsymbol{\omega}_m \times (\mathbf{I}_m \boldsymbol{\omega}_m) \end{bmatrix} + \begin{bmatrix} m_m(0, g, 0)^T + \mathbf{F}_e \\ \mathbf{M}_e \end{bmatrix} &= \begin{bmatrix} \sum_{i=1}^n (T_i \hat{\mathbf{u}}_i) + \sum_{j=1}^m (F_j \hat{\mathbf{v}}_j) \\ \sum_{i=1}^n (T_i \mathbf{r}_i \times \hat{\mathbf{u}}_i) + \sum_{j=1}^m (F_j \mathbf{c}_j \times \hat{\mathbf{v}}_j) \end{bmatrix} \\
&= \begin{bmatrix} \hat{\mathbf{u}}_1 & \hat{\mathbf{u}}_2 & \cdots & \hat{\mathbf{u}}_n \\ \mathbf{r}_1 \times \hat{\mathbf{u}}_1 & \mathbf{r}_2 \times \hat{\mathbf{u}}_2 & \cdots & \mathbf{r}_n \times \hat{\mathbf{u}}_n \\ \hat{\mathbf{v}}_1 & \hat{\mathbf{v}}_2 & \cdots & \hat{\mathbf{v}}_m \\ \mathbf{c}_1 \times \hat{\mathbf{v}}_1 & \mathbf{c}_2 \times \hat{\mathbf{v}}_2 & \cdots & \mathbf{c}_m \times \hat{\mathbf{v}}_m \end{bmatrix} \begin{bmatrix} \mathbf{T} \\ \mathbf{F} \end{bmatrix} \\
&= \mathbf{J}^T \begin{bmatrix} \mathbf{T} \\ \mathbf{F} \end{bmatrix}, \tag{14}
\end{aligned}$$

where $\mathbf{T} \triangleq [T_1, T_2, \dots, T_n]$ is the cable tension vector of the CDPR. $\mathbf{F} \triangleq [F_1, F_2, \dots, F_m]$ represent the cable tension vector from auxiliary fixed pulleys. \mathbf{F}_e and \mathbf{M}_e are external forces and moments, respectively. Then, Eq. (14) can be arranged as

$$\underbrace{\begin{bmatrix} m_m \\ \mathbf{I}_m \end{bmatrix}}_{\triangleq \mathbf{M}} \underbrace{\begin{bmatrix} \dot{\mathbf{v}}_m \\ \dot{\boldsymbol{\omega}}_m \end{bmatrix}}_{\triangleq \dot{\mathbf{q}}} + \underbrace{\begin{bmatrix} \mathbf{0} \\ \boldsymbol{\omega}_m \times (\mathbf{I}_m \boldsymbol{\omega}_m) \end{bmatrix}}_{\triangleq \mathbf{C}(\mathbf{q}, \dot{\mathbf{q}}) \dot{\mathbf{q}}} + \underbrace{\begin{bmatrix} m_m(0, g, 0)^T \\ \mathbf{0} \end{bmatrix}}_{\triangleq \mathbf{G}(\mathbf{q})} + \begin{bmatrix} \mathbf{F}_e \\ \mathbf{M}_e \end{bmatrix} = \mathbf{J}^T \begin{bmatrix} \mathbf{T} \\ \mathbf{F} \end{bmatrix}, \tag{15}$$

where \mathbf{q} , $\dot{\mathbf{q}}$, $\ddot{\mathbf{q}}$ represent the vectors of generalized coordinates, velocities, and accelerations, respectively. \mathbf{M} denotes the inertia matrix, $\mathbf{C}(\mathbf{q}, \dot{\mathbf{q}})$ represents the combined Coriolis and centripetal matrix, and $\mathbf{G}(\mathbf{q})$ denotes the gravitational vector, respectively.

3. Workspace Analysis Method

To analyze the workspace, here, we ignore external force \mathbf{F}_e and moment \mathbf{M}_e for simplification. For an arbitrary equilibrium point, i.e., $\ddot{\mathbf{q}} = \dot{\mathbf{q}} = \mathbf{0}$, Eq. (13) can be simplified as

$$\mathbf{G}(\mathbf{q}) = \mathbf{J}^T \begin{bmatrix} \mathbf{T} \\ \mathbf{F} \end{bmatrix} = \begin{bmatrix} \mathbf{J}_l^T & \mathbf{J}_d^T \end{bmatrix} \begin{bmatrix} \mathbf{T} \\ \mathbf{F} \end{bmatrix} = \mathbf{J}_l^T \mathbf{T} + \mathbf{J}_d^T \mathbf{F}. \tag{16}$$

Defining $\mathbf{u} \triangleq \mathbf{G}(\mathbf{q}) - \mathbf{J}_d^T \mathbf{F}$ as an input vector, then we get

$$\mathbf{u} = \mathbf{G}(\mathbf{q}) - \mathbf{J}_d^T \mathbf{F} = \mathbf{J}_l^T \mathbf{T}. \tag{17}$$

For a general case, Eq. (17) with constraints can be arranged as

$$\mathbf{T} = (\mathbf{J}_l^T)^+ \mathbf{u} + \alpha \text{Null}(\mathbf{J}_l^T), \quad 0 < T_{i \min} \leq T_i \leq T_{i \max}, \tag{18}$$

where $(\mathbf{J}_l^T)^+$ and $\text{Null}(\mathbf{J}_l^T)$ represent pseudoinverse and null space of matrix \mathbf{J}_l^T , respectively. α denotes a variable that can adjust \mathbf{T} to satisfy with the constraints [33]. Eq. (18) provides a genetic approach, but there may exist multi solutions and it is not easy to solve this problem for different robot configurations by using (18). For the configuration in Section 3, we propose another more effective method which can find a unique solution (let the rotation of the moving platform be zero). First, suppose

$$\mathbf{A}_l = [\mathbf{A}_{l1}, \mathbf{A}_{l2}, \mathbf{A}_{l3}, \mathbf{A}_{l4}] \triangleq \mathbf{J}_l^T, \tag{19}$$

where \mathbf{A}_{i1} is the sub-vector of \mathbf{A}_i . In addition, the redundancy resolution problem resulting from multi-cables can be solved as follows: since the equivalent four-cable planar CDPR has one DOR, then is redefined as a new 3×4 matrix. One can restrict one of cable tensions T_i ($i = 1, 2, 3, 4$) to the maximum allowable value $T_{i \max}$. In this case, the redundancy resolution and cable tensions are described as

$$\begin{cases} [T_2, T_3, T_4]^T = [\mathbf{A}_{i2}, \mathbf{A}_{i3}, \mathbf{A}_{i4}]^{-1}(\mathbf{u} - \mathbf{A}_{i1}T_{1 \max}), & \text{for } T_1 = T_{1 \max} \\ [T_1, T_3, T_4]^T = [\mathbf{A}_{i1}, \mathbf{A}_{i3}, \mathbf{A}_{i4}]^{-1}(\mathbf{u} - \mathbf{A}_{i2}T_{2 \max}), & \text{for } T_2 = T_{2 \max} \\ [T_1, T_2, T_4]^T = [\mathbf{A}_{i1}, \mathbf{A}_{i2}, \mathbf{A}_{i4}]^{-1}(\mathbf{u} - \mathbf{A}_{i3}T_{3 \max}), & \text{for } T_3 = T_{3 \max} \\ [T_1, T_2, T_3]^T = [\mathbf{A}_{i1}, \mathbf{A}_{i2}, \mathbf{A}_{i3}]^{-1}(\mathbf{u} - \mathbf{A}_{i4}T_{4 \max}), & \text{for } T_4 = T_{4 \max} \end{cases} \quad (20)$$

Eq. (20) includes four solutions without constraints. Combining these solutions and constraints of cables, we define the cost function (cables are assumed to be no elastic) as

$$\begin{aligned} \Gamma &= \max \left\{ \|\mathbf{T}_{\text{opt1}}\|, \|\mathbf{T}_{\text{opt2}}\|, \|\mathbf{T}_{\text{opt3}}\|, \|\mathbf{T}_{\text{opt4}}\| \right\} \\ \text{s.t. } \mathbf{T}_{\text{opt1}} &= [T_{1 \max}, T_2, T_3, T_4]^T \\ \mathbf{T}_{\text{opt2}} &= [T_1, T_{2 \max}, T_3, T_4]^T \\ \mathbf{T}_{\text{opt3}} &= [T_1, T_2, T_{3 \max}, T_4]^T \\ \mathbf{T}_{\text{opt4}} &= [T_1, T_2, T_3, T_{4 \max}]^T \\ 0 &\leq T_{k \min} \leq T_k \leq T_{k \max}, \quad k = 1, 2, 3, 4, 5, \end{aligned} \quad (21)$$

where Γ denotes the maximum stiffness of the CDPR. Clearly, after obtaining Γ , we can also get the corresponding optimal cable tension vector $\mathbf{T}_{\text{opt}}^*$ ($\mathbf{T}_{\text{opt}i}^*$, $i = 1, 2, 3, 4$). From (17), (19), (20), and (21), we know that $\mathbf{T}_{\text{opt}}^*$ is a function in terms of $\mathbf{p}(x, y)$, w_p and \mathbf{F} . Since \mathbf{F} is a vector including two elements (they are equal to each other), here, we use T_5 to represent one element. Then, for a desired position (x, y) , we can verify the reachability of this point using $\mathbf{T}_{\text{opt}}^*(w_p, T_5)$. w_p and T_5 are position and force parameters to optimize the reachable workspace. We can also obtain more conclusions: given x, y , and w_p , $\mathbf{T}_{\text{opt}}^*(w_p, T_5)$ and T_5 are linear relative. In comparison with the method shown in [16], Eqs. (20) and (21) can ensure that all the cable tensions are positive. If cables are elastic, we can introduce cable length constraints into (21):

$$\begin{aligned} \Gamma &= \max \left\{ \|\mathbf{T}_{\text{opt1}}\|, \|\mathbf{T}_{\text{opt2}}\|, \|\mathbf{T}_{\text{opt3}}\|, \|\mathbf{T}_{\text{opt4}}\| \right\} \\ \text{s.t. } \mathbf{T}_{\text{opt1}} &= [T_{1 \max}, T_2, T_3, T_4]^T \\ \mathbf{T}_{\text{opt2}} &= [T_1, T_{2 \max}, T_3, T_4]^T \\ \mathbf{T}_{\text{opt3}} &= [T_1, T_2, T_{3 \max}, T_4]^T \\ \mathbf{T}_{\text{opt4}} &= [T_1, T_2, T_3, T_{4 \max}]^T \\ 0 &\leq T_{k \min} \leq T_k \leq T_{k \max}, \quad k = 1, 2, 3, 4, 5 \\ 0 &\leq l_{0k \min} \leq \frac{l_k EA_k}{T_k + EA_k} \leq l_{0k \max}, \quad k = 1, 2, 3, 4, 5, \end{aligned} \quad (22)$$

where EA_k represents the product of the modulus of elasticity and cross-sectional area of the k -th cable, and l_k denotes k -th cable length. $l_{0k \min}$ and $l_{0k \max}$ are the minimum and maximum length of the k -th unstretched cable.

Additionally, we propose Algorithm 1 to find the reachable workspace. Given the desired x, y , and T_5 and follow the steps in Algorithm 1, we can obtain a set of feasible position (x, y) named reachable workspace. $x_{\min}, x_{\max}, y_{\min}, y_{\max}$ are kinematic constraints. In this paper, they are provided in Table 1 for case studies.

4. Numerical Results and Discussion

In this section, we conduct different scenarios for workspace analysis via the proposed models (in Section 2) and algorithms (in Section 3). First, we provide a planar CDPR, which is actuated by four cables (see Figure 2). All cables are assumed to be straight, massless, and non-elastic. In order to achieve the goal of workspace expansion and parameter optimization, we introduce one or more fixed pulleys on the mobile platform. Here, we propose four possible configurations for comparison (see Figure 2). In Figure 2, the arrangement of the cables are different, in which mounting a single pulley on the top side of the platform, mounting two pulleys on the top side of the platform, mounting two pulleys on the bottom side of the platform, and mounting two pulleys on the top side of

Algorithm 1 Calculation of reachable workspace.

Input: Given the desired x and y and T_5 .

Output: Reachable workspace x, y .

 ▶ Position $\mathbf{p}(x, y)$.

- 1: Given desired workspace $x_{\min}, x_{\max}, y_{\min}, y_{\max}$, and a set of T_5 ; ▶ $x_{\min}, x_{\max}, y_{\min}, y_{\max}$ are kinematic constraints.
 - 2: **for** x_{\min} to x_{\max} **do**
 - 3: **for** y_{\min} to y_{\max} **do**
 - 4: Using (13) and (12) to find \mathbf{J}_l and \mathbf{J}_d , respectively;
 - 5: Using (17) to find \mathbf{u} ;
 - 6: Substituting \mathbf{u} and \mathbf{J}_l into (19) and (20);
 - 7: Recording the current x, y if (21) or (22) holds;
 - 8: **end for**
 - 9: **end for**
 - 10: **Return** Reachable workspace x, y .
-

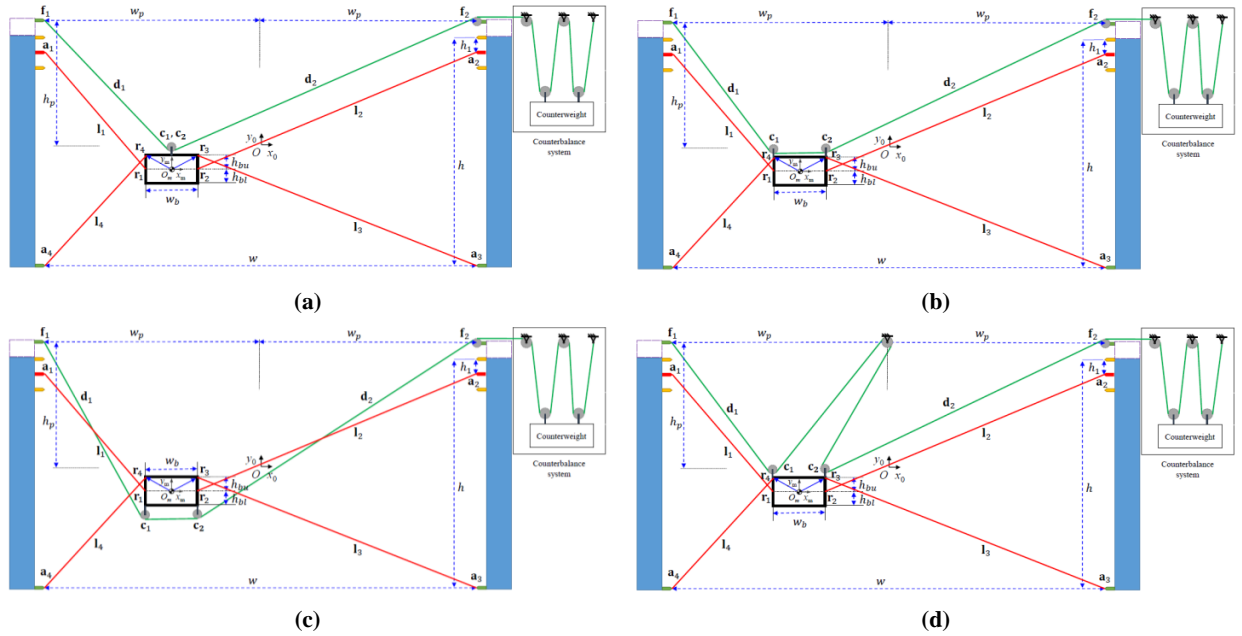


Figure 2: Possible robot configurations and coordinates assignment. (a) Mounting a single pulley on the top side of the platform. (b) Mounting two pulleys on the top side of the platform. (c) Mounting two pulleys on the bottom side of the platform. (d) Mounting two pulleys on the top side of the platform and one fixed pulley on the static frame.

the platform and one fixed pulley on the static frame are shown in Figure 2 (a)-(d), respectively. We can also add more numbers of auxiliary fixed pulleys (i.e., greater than two), but we found that other configurations do not help increase the reachable workspace. In this paper, we focus on one of them, i.e., Figure 2 (a), for detailed analysis and case studies. Besides, in Figure 2 (a), the coordinate assignment of the proposed CDP are given, with geometrical dimensions $w, h, w_b, w_p, h_p, h_{bp}, w_{bp}, h_{bu}$, and h_{bl} . The global coordinate frame X_0OY_0 is located at the center of the static frame. Two points \mathbf{c}_1 and \mathbf{c}_2 connected to auxiliary fixed pulleys \mathbf{f}_1 and \mathbf{f}_2 are located at the top center of the platform. The following vectors are defined as: $\mathbf{r}_1 = [-w_b/2, h_{bl}, 0]^T$, $\mathbf{r}_2 = [w_b/2, h_{bl}, 0]^T$, $\mathbf{r}_3 = [w_b/2, -h_{bl}, 0]^T$, $\mathbf{r}_4 = [-w_b/2, -h_{bl}, 0]^T$, $\mathbf{c}_1 = [-w_{bp}/2, h_{bp}, 0]^T$, $\mathbf{c}_2 = [w_{bp}/2, h_{bp}, 0]^T$, $\mathbf{a}_1 = [-w/2, h/2, 0]^T$, $\mathbf{a}_2 = [w/2, h/2, 0]^T$, $\mathbf{a}_3 = [w/2, -h/2, 0]^T$, $\mathbf{a}_4 = [-w/2, -h/2, 0]^T$, $\mathbf{f}_1 = [-w_p, h_p, 0]^T$, $\mathbf{f}_2 = [0, h_p, 0]^T$, $\mathbf{f}_3 = [0, h_p, 0]^T$, and $\mathbf{f}_4 = [w_p, h_p, 0]^T$. Using the specific parameters $w, h, w_b, w_p, h_p, h_{bp}, w_{bp}, h_{bu}$, and h_{bl} provided in Table 1, we can obtain the vectors above. Substituting these vectors in to the equations in Section 2 and Section 3, we can find the corresponding items (in (16), (17), and (19)) as below:

Table 1: Parameters for case studies.

Symbol	Value	Symbol	Value
w	28.0 m	h_p	3.246 m
h	5.70 m	h_{bp}	0.45 m
w_b	1.90 m	w_{bp}	0.95 m
h_1	0.45 m	h_{bu}	0.45 m
$[x_{\min}, x_{\max}]$	$[-12.5, 12.5]$ m	$[y_{\min}, y_{\max}]$	$[-2.85, 2.15]$ m
m_m	300 kg	g	9.81 m/s ²
$T_{1 \max}, T_{2 \max}, T_{5 \max}$	16 000 N	$T_{3 \max}, T_{4 \max}$	12 000 N
$T_{k \min}, k = 1, 2, 3, 4, 5$	0 N		

$$\mathbf{G}(\mathbf{q}) = [0, m_m g, 0]^T, \quad (23)$$

where m_m denotes the mass of the moving platform.

$$\mathbf{F} = [T_5, T_5], \quad (24)$$

where T_5 represents the cable tension connected to a fixed pulley for optimal design. The structure matrix and Jacobian matrix are described as

$$\mathbf{A}_l = \begin{pmatrix} -\frac{w-w_b+2x}{2\chi} & -\frac{w_b-w+2x}{2\chi} & -\frac{w_b-w+2x}{2\delta} & -\frac{w-w_b+2x}{2\delta} \\ -\frac{h_1-\frac{h}{2}+y}{\chi} & -\frac{h_1-\frac{h}{2}+y}{\chi} & -\frac{\frac{h}{2}+h_{bu}+y}{\delta} & -\frac{\frac{h}{2}+h_{bu}+y}{\delta} \\ \frac{w_b(h_1-\frac{h}{2}+y)}{2\chi} & -\frac{w_b(h_1-\frac{h}{2}+y)}{2\chi} & -\frac{2h_{bu}w+hwb-4h_{bu}x+2wby}{4\delta} & \frac{2h_{bu}w+hwb+4h_{bu}x+2wby}{4\delta} \end{pmatrix}, \quad (25)$$

and

$$\mathbf{J}_d = \begin{pmatrix} -\frac{w_p+x}{\eta} & \frac{w_p-x}{\kappa} \\ -\frac{h_{bp}-h_p+y}{\eta} & -\frac{h_{bp}-h_p+y}{\kappa} \\ \frac{h_{bp}(w_p+x)}{\eta} & -\frac{h_{bp}(w_p-x)}{\kappa} \end{pmatrix}^T, \quad (26)$$

with $\chi = \sqrt{(h_1 - \frac{h}{2} + y)^2 + (\frac{w}{2} - \frac{w_b}{2} + x)^2}$, $\delta = \sqrt{(\frac{h}{2} + h_{bu} + y)^2 + (\frac{w_b}{2} - \frac{w}{2} + x)^2}$, $\eta = \sqrt{(w_p + x)^2 + (h_{bp} - h_p + y)^2}$, and $\kappa = \sqrt{(w_p - x)^2 + (h_{bp} - h_p + y)^2}$. w_b is the other parameter (see Figure 2) for optimization. Substituting (23)-(26) back into (20)-(21) and using Algorithm 1, we conduct the scenarios of workspace analysis and optimal design as follows:

4.1. Scenario 1: Choosing w_p

In this scenario, we change the parameter w_p to estimate the impact to the reachable workspace. Here, we conduct different conditions and let T_5 be 1000 N, 2000 N, 3000 N, 4000 N, and 5000 N for analysis. In each condition, T_5 is constant and the objective is find the optimal w_p . By carrying out Algorithm 1, we can obtain the results shown in Figure 3. It is clear that w_p equaling 13 m is a proper value that makes the area of reachable workspace be the largest.

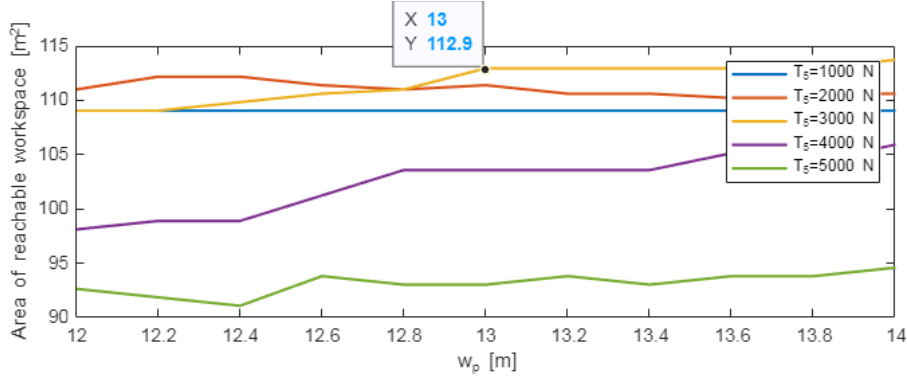


Figure 3: Area of reachable workspace versus w_p .

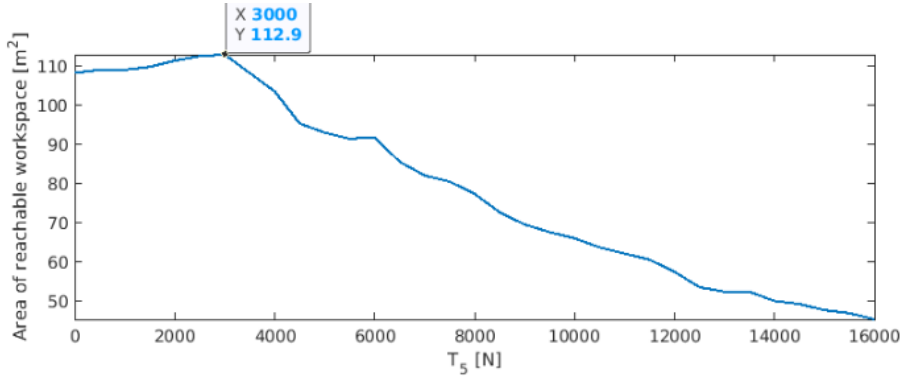


Figure 4: Area of reachable workspace versus T_5 .

4.2. Scenario 2: Choosing T_5

In Subsection 4.1, we obtained the proper value of w_p (13 m). Applying this value, we conduct a new scenario: changing T_5 to estimate its effect on the reachable workspace, and the result is shown in Figure 4. The result reveals that when T_5 is equal to 3000 N, the workspace reaches the peak point, i.e., the optimal value. Increasing T_5 does not improve the reachable workspace. After obtaining T_5 , the counterweight M can be computed as $M = \zeta T_5$, where ζ represents the number of cables in the counterbalance system.

4.3. Discussion: Desired Workspace versus Reachable Workspace

In Subsection 4.1 and Subsection 4.2, we obtained the optimal w_p (13 m) and T_5 (3000 N) by maximizing the area of the reachable workspace. In actual system design, we are also interested in the surface of the workspace, e.g., the corner of the workspace. Here, we use an example of reachable workspace compared with the desired workspace (see Figure 5) to illustrate this point. In Figure 5, the results show that larger T_5 can increase reachable workspace on the top, but lose the reachable workspace on the bottom, especially on the bottom left and right. When T_5 is equal to 3000 N, the area of reachable workspace is the largest (112.9 m²); when T_5 equals 2000 N, the area of the reachable workspace (112.9 m²) is smaller but the corners on the bottom can be covered. Hence, in real system design, we can choose the value of T_5 between 2000 N and 3000 N regarding the specific need. Ideally, we can use a hydraulic system to adjust T_5 to satisfy with maximizing the area of the workspace as well as covering the corners of the desired workspace.

4.4. Discussion: Comparison of Different Robot Configurations

Figure 2 provided four possible configurations, and then we focused on the one shown in Figure 2(a) for detailed workspace expansion and parameter optimization. To compare the corresponding results with those of other confi-

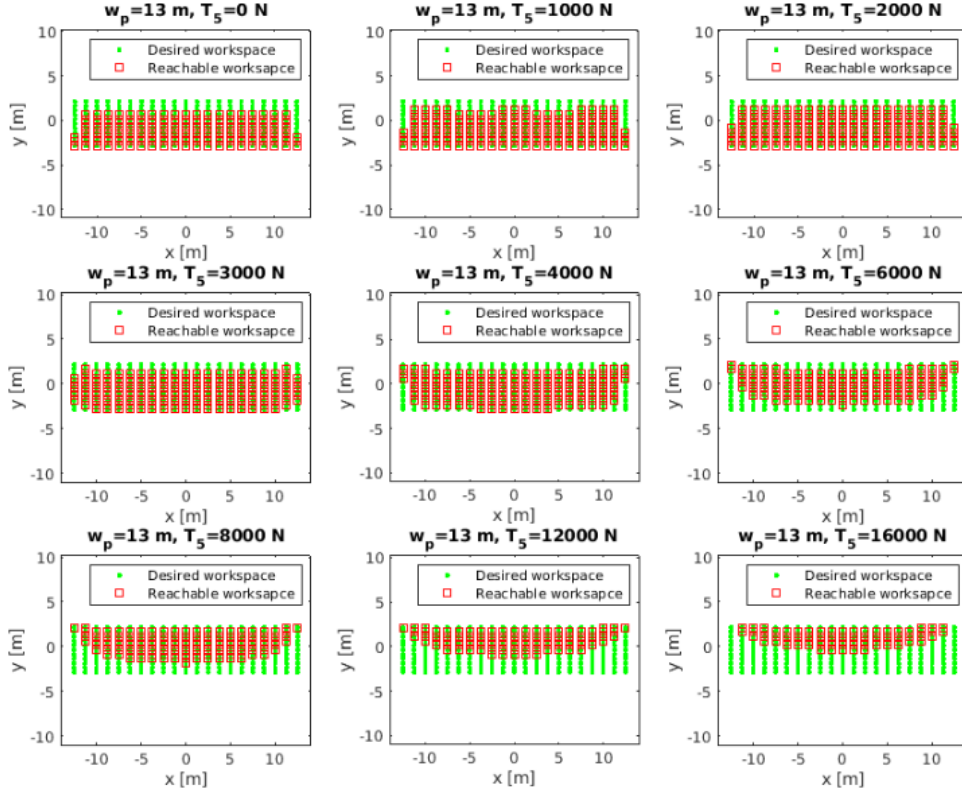


Figure 5: Desired workspace versus reachable workspace.

urations, we also conduct the following cases: To begin with, the area of reachable workspace of another three robot configurations are provided in Figure 6, in which Figure 6 (a), (b), and (c) correspond to the configurations shown in Figure 2 (b), (c), and (d), respectively. Here, we use w_p that is equal to 13 m and the scope of T_5 in all cases for easy comparison. Clearly, in comparison with the result shown in Figure 4, when T_5 is equal to 3000 N, the areas of reachable workspace in Figure 6 are all less than that of Figure 4. Additionally, Figure 6 (b) also shows a large area of workspace, but the cables (green lines in Figure 2) between the moving and fixed pulleys may collide with the platform and other cables (red lines in Figure 2). Figure 6 (c) shows that increasing the number of fixed pulleys does not contribute to the workspace maximum. In short, targeting the workspace maximum, the configuration shown in Figure 2 (a) is the optimal one (considering the collisions between the platform and cables), and we have 4.34% increase in the reachable workspace.

Moreover, the results of the desired workspace versus the reachable workspace of another three robot configurations are provided in Figure 7, in which Figure 7 (a), (b), and (c) correspond to the configurations shown in Figure 2 (b), (c), and (d), respectively. Compared to the result shown in Figure 5, we can indicate conclusions as follows: Clearly, Figure 7 (a) shows a smaller available workspace. Without considering collisions between the moving platform and cables, Figure 7 (b) shows a larger vertical feasible workspace to reach the top position of the desired workspace. Figure 7 (c) can enlarge the vertical space with a smaller T_5 (e.g., at T_5 equals 1000 N), but the corners are not reached. In summary, regarding the results shown in Figure 5, Figure 6, and Figure 7, we can conclude that the configuration shown in Figure 2 (a) is the optimal configuration (aim to maximize the workspace) if collisions are considered; if the collisions are not considered or can be avoided through mechanism design, the configuration shown in Figure 6 (b) is the optimal one.

4.5. Discussion: Active Control of T_5

In Subsection 4.2, we considered T_5 as a parameter for workspace improvement and obtained the optimal value. In this scenario, we consider T_5 as a variable, i.e., replacing the counterweight by a hydraulic system so that T_5 is

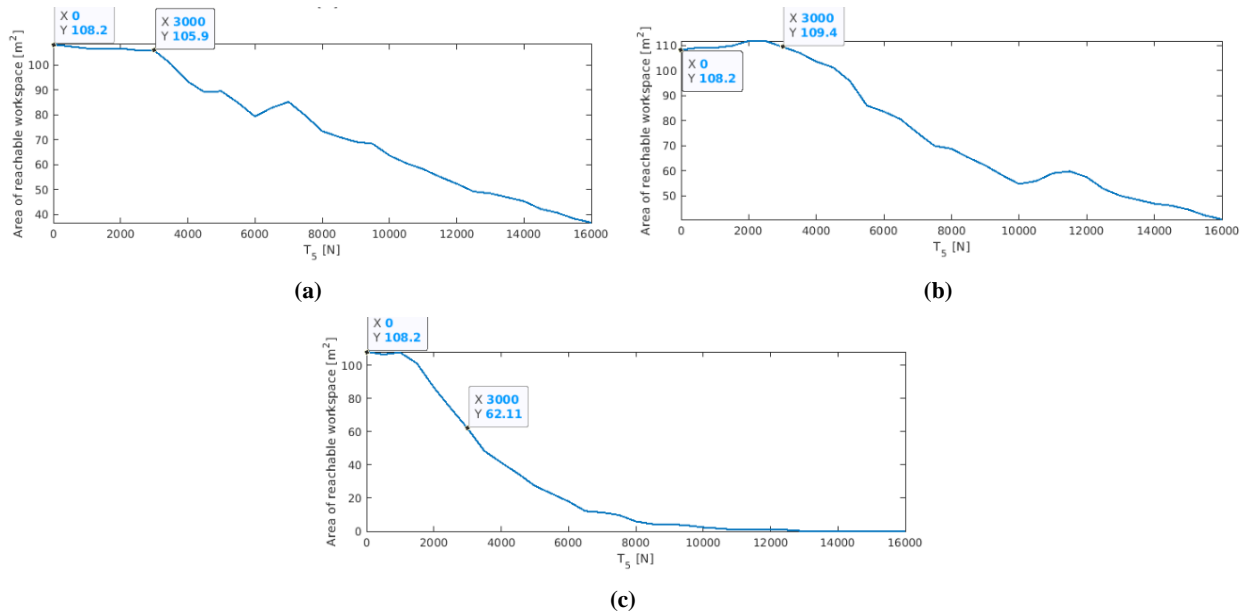


Figure 6: Area of reachable workspace of different robot configurations versus T_5 . (a) Responses of the configuration Figure 2 (b). (b) Responses of the configuration Figure 2 (c). (c) Responses of the configuration Figure 2 (d).

a control input. In this case, it is interesting to adjust T_5 to evaluate whether the reachable workspace can cover the desired workspace. Here, the constraint of $T_{5\max}$ (16000 N) is not included to show the maximum coverage of workspace. Using the obtained w_p in Subsection 4.1 and the configuration in Figure 2 (a), we conduct this scenario. The results of workspace versus T_5 are provided in Figure 8, in which Figure 8 (a)-(d) show T_5 is equal to 0-5000 N, 0-10000 N, 0-20000 N, and 0-26000 N, respectively. Clearly, the broader region of T_5 results in a larger reachable workspace, and the desired workspace can be covered entirely (see Figure 8 (d)).

5. Conclusions and Future Work

In this paper, we introduced workspace analysis and optimal design of cable-driven parallel robots through auxiliary counterbalances. Based on the proposed workspace analysis algorithm, different robot configurations and numerical results were developed for parameters optimization and reachable workspace was increased. Using the proposed approach we had 4.34% increase in the reachable workspace. Numerical results in different aspects also suggested the effectiveness of the aforementioned approach. In the further, we plan to use the optimal parameters for real system design.

Acknowledgment

The authors would like to acknowledge the financial support of the Natural Sciences and Engineering Research Council of Canada (NSERC).

References

- [1] N. G. Dagalakis, J. S. Albus, et al., Stiffness Study of a Parallel Link Robot Crane for Shipbuilding Applications, *J. Offshore Mech. Arct. Eng.* 111 (1989) 183–193. doi:10.1115/1.3257146.
- [2] J. Albus, R. Bostelman, N. Dagalakis, The NIST SPIDER, A Robot Crane, *J. Res. Natl. Inst. Stand. Technol.* 97 (3) (1992) 373–385. doi:10.6028/jres.097.016.

- [3] S. J. T. Méndez, Low Mobility Cable Robot with Application to Robotic Warehousing, Ph.D. thesis, University of Waterloo, Waterloo, ON, Canada (2014).
- [4] H. Jamshidifar, A. Khajepour, B. Fidan, M. Rushton, Vibration regulation of kinematically constrained cable-driven parallel robots with minimum number of actuators, *IEEE/ASME Trans. Mechatronics* 25 (1) (2020) 21–31. doi:10.1109/TMECH.2019.2946780.
- [5] H. Jamshidifar, Integrated Trajectory-Tracking and Vibration Control of Kinematically-Constrained Warehousing Cable Robots, Ph.D. thesis, University of Waterloo, Waterloo, ON, Canada (2018).
- [6] R. Qi, A. Khajepour, W. W. Melek, Generalized Flexible Hybrid Cable-Driven Robot (HCDR): Modeling, Control, and Analysis, arXiv:1911.06222 (2019).
- [7] R. Qi, Redundant Hybrid Cable-Driven Robots: Modeling, Control, and Analysis, Ph.D. thesis, University of Waterloo, Waterloo, ON, Canada (2018).
- [8] T. Arai, S. Matsumura, et al., A proposal for a wire suspended manipulator: A kinematic analysis, *Robotica* 17 (1) (1999) 3–9. doi:10.1017/S0263574799000995.
- [9] H. Osumi, Y. Utsugi, M. Koshikawa, Development of a manipulator suspended by parallel wire structure, in: Proc. IEEE/RSJ Int. Conf. Intell. Robots Syst., Takamatsu, Japan, 2000, pp. 498–503. doi:10.1109/IR0S.2000.894653.
- [10] M. Bamdad, F. Taheri, N. Abtahi, Dynamic analysis of a hybrid cable-suspended planar manipulator, in: Proc. IEEE Int. Conf. Robot. Autom., Seattle, Washington, USA, 2015, pp. 1621–1626. doi:10.1109/ICRA.2015.7139405.
- [11] M. Gouttefarde, Static Analysis of Planar 3-DOF Cable-Suspended Parallel Robots Carrying a Serial Manipulator, in: P. Wenger, P. Flores (Eds.), *New Trends Mechanism Machine Sci.*, Springer Int. Publishing, Cham, 2017, pp. 363–371.
- [12] J. S. Albus, Cable Arrangement and Lifting Platform for Stabilized Load Lifting, U.S. Patent 4,883,184, Nov. 28, 1989.
- [13] J. S. Albus, R. V. Bostelman, A. S. Jacoff, Modular Suspended Manipulator, U.S. Patent 6,566,834 B1, May 20, 2003.
- [14] Spidercam GmbH, Spidercam, [Accessed: Dec. 16, 2020]. [Online]. Available: <https://www.spidercam.tv>.
- [15] SKYCAM LLC, Skycam, [Accessed: Dec. 16, 2020]. [Online]. Available: <http://www.skycam.tv>.
- [16] M. Rushton, Vibration Control in Cable Robots Using a Multi-Axis Reaction System, Master's thesis, University of Waterloo, Waterloo, ON, Canada (2016).
- [17] P. R. Pagilla, B. Yu, An experimental study of planar impact of a robot manipulator, *IEEE/ASME Trans. Mechatronics* 9 (1) (2004) 123–128. doi:10.1109/TMECH.2004.823888.
- [18] D. Lau, D. Oetomo, S. K. Halgamuge, Generalized modeling of multilink cable-driven manipulators with arbitrary routing using the cable-routing matrix, *IEEE Trans. Robot.* 29 (5) (2013) 1102–1113. doi:10.1109/TR0.2013.2264866.
- [19] N. Mostashiri, J. S. Dhupia, et al., A Review of Research Aspects of Redundantly Actuated Parallel Robots for Enabling Further Applications, *IEEE/ASME Trans. Mechatronics* 23 (3) (2018) 1259–1269.
- [20] C. Viegas, M. Tavakoli, et al., SCALA—A Scalable Rail-based Multirobot System for Large Space Automation: Design and Development, *IEEE/ASME Trans. Mechatronics* 22 (5) (2017) 2208–2217. doi:10.1109/TMECH.2017.2740723.
- [21] H. D. Taghirad, Y. B. Bedoustani, An analytic-iterative redundancy resolution scheme for cable-driven redundant parallel manipulators, *IEEE Trans. Robot.* 27 (6) (2011) 1137–1143. doi:10.1109/TR0.2011.2163433.
- [22] Z. Mu, H. Yuan, W. Xu, T. Liu, B. Liang, A segmented geometry method for kinematics and configuration planning of spatial hyper-redundant manipulators, *IEEE Trans. Syst. Man Cybern. Syst.* 50 (5) (2020) 1746–1756. doi:10.1109/TSMC.2017.2784828.
- [23] M. J. Otis, S. Perreault, et al., Determination and management of cable interferences between two 6-dof foot platforms in a cable-driven locomotion interface, *IEEE Trans. Syst. Man Cybern. A Syst. Hum.* 39 (3) (2009) 528–544. doi:10.1109/TSMCA.2009.2013188.
- [24] M. Chen, Y. Ren, J. Liu, Antidisturbance control for a suspension cable system of helicopter subject to input nonlinearities, *IEEE Trans. Syst. Man Cybern. Syst.* 48 (12) (2018) 2292–2304. doi:10.1109/TSMC.2017.2710638.
- [25] C. B. Pham, S. H. Yeo, G. Yang, Workspace analysis and optimal design of cable-driven planar parallel manipulators, in: Proc. IEEE Int. Conf. Robot. Autom. Mechatronics, Singapore, 2004, pp. 219–224. doi:10.1109/RAMECH.2004.1438920.
- [26] Y. Li, Q. Xu, Ga-based multi-objective optimal design of a planar 3-dof cable-driven parallel manipulator, in: Proc. IEEE Int. Conf. Robot. Biomimetics, Kunming, China, 2006, pp. 1360–1365. doi:10.1109/ROBIO.2006.340127.
- [27] J. Bolboli, M. A. Khosravi, F. Abdollahi, Stiffness feasible workspace of cable-driven parallel robots with application to optimal design of a planar cable robot, *Robot. Auton. Syst.* 114 (2019) 19–28. doi:<https://doi.org/10.1016/j.robot.2019.01.012>.
- [28] X. Tang, L. Tang, J. Wang, et al., Workspace quality analysis and application for a completely restrained 3-dof planar cable-driven parallel manipulator, *J. Mech. Sci. Technol.* 27 (8) (2013) 2391–2399. doi:<https://doi.org/10.1007/s12206-013-0624-7>.
- [29] J. Pusey, A. Fattah, S. Agrawal, E. Messina, Design and workspace analysis of a 6–6 cable-suspended parallel robot, *Mech. Mach. Theory* 39 (7) (2004) 761–778. doi:<https://doi.org/10.1016/j.mechmachtheory.2004.02.010>.
- [30] J.-P. Merlet, On the workspace of suspended cable-driven parallel robots, in: Proc. IEEE Int. Conf. Robot. Autom., Stockholm, Sweden, 2016, pp. 841–846. doi:10.1109/ICRA.2016.7487214.
- [31] Q. Duan, V. Vashista, S. K. Agrawal, Effect on wrench-feasible workspace of cable-driven parallel robots by adding springs, *Mech. Mach. Theory* 86 (2015) 201–210. doi:<https://doi.org/10.1016/j.mechmachtheory.2014.12.009>.
- [32] S. R. Oh, S. K. Agrawal, Cable suspended planar robots with redundant cables: controllers with positive tensions, *IEEE Trans. Robot.* 21 (3) (2005) 457–465. doi:10.1109/TR0.2004.838029.
- [33] S. Behzadipour, Ultra-High-Speed Cable-Based Robots, Ph.D. thesis, University of Waterloo, Waterloo, ON, Canada (2005).

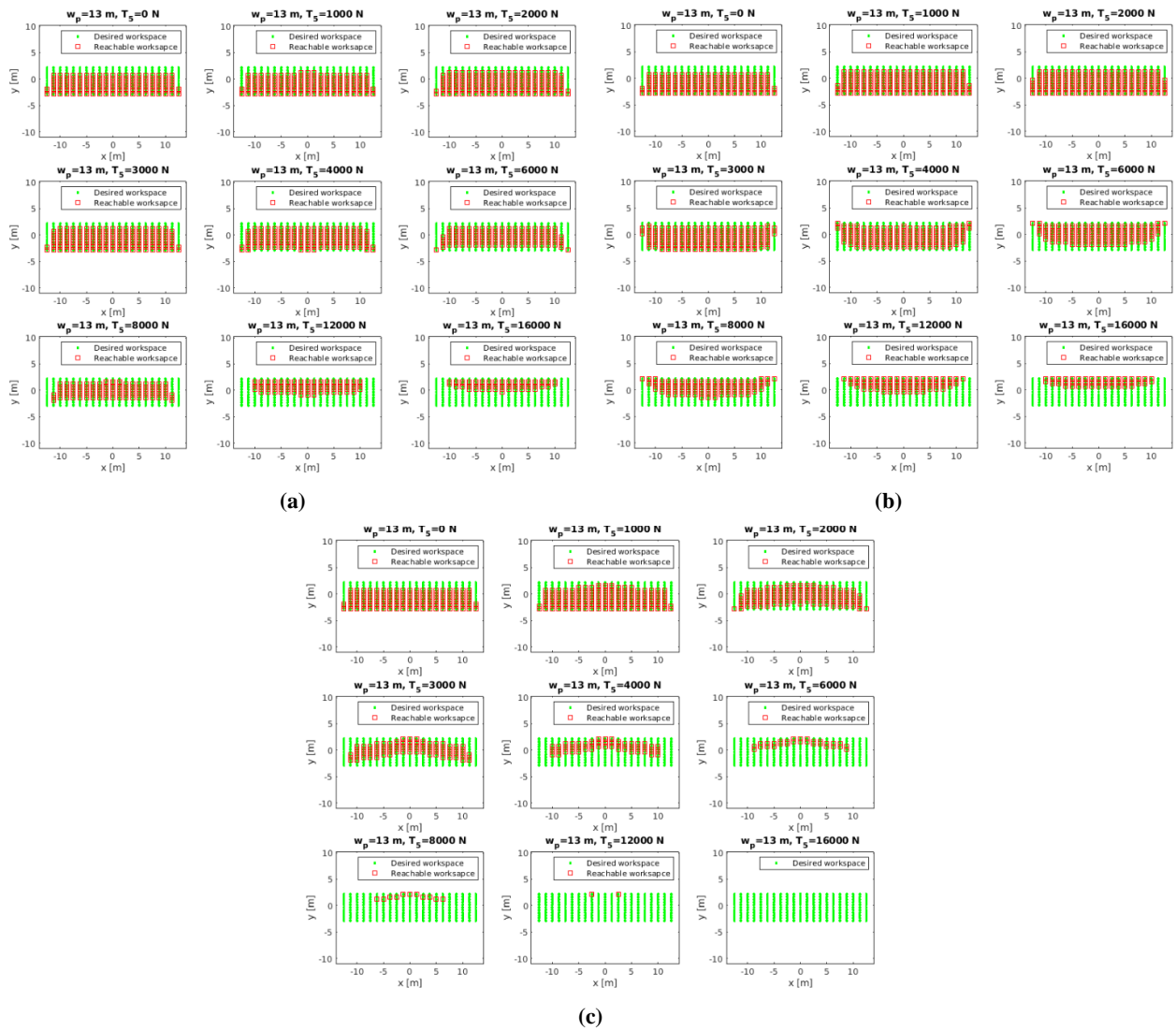


Figure 7: Desired workspace versus reachable workspace of different robot configurations. (a) Responses of the configuration Figure 2 (b). (b) Responses of the configuration Figure 2 (c). (c) Responses of the configuration Figure 2 (d).

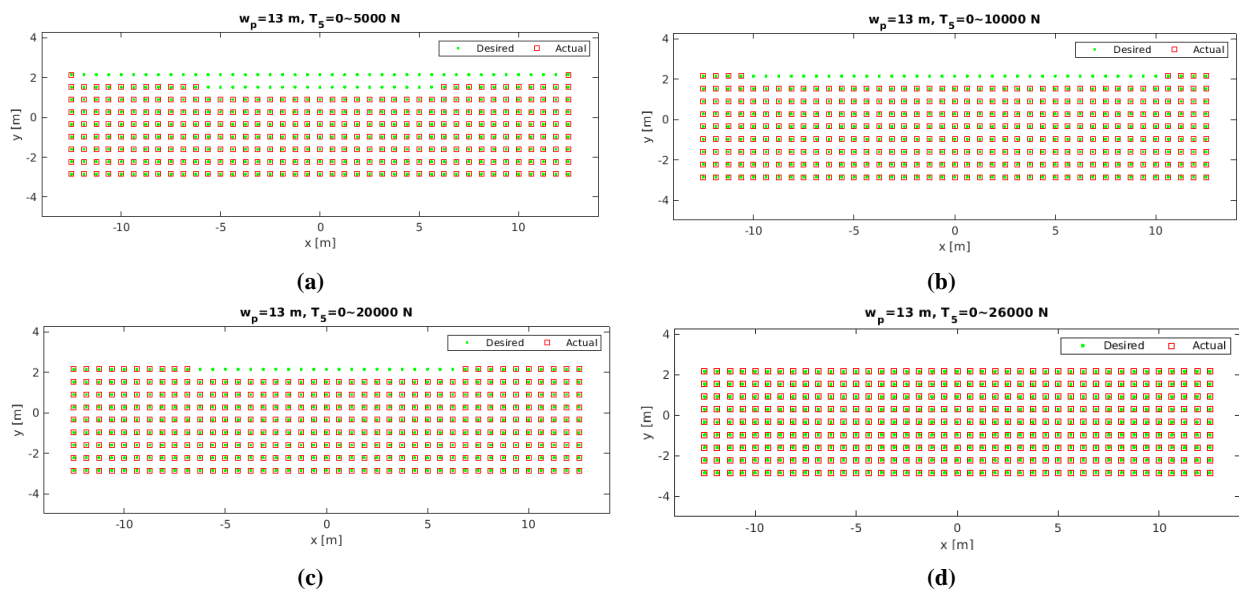


Figure 8: Desired workspace versus reachable workspace with the active control of T_5 . (a) $T_5 = 0-5000$ N. (b) $T_5 = 0-10000$ N. (c) $T_5 = 0-20000$ N. (d) $T_5 = 0-26000$ N.